An Approximate Footprint Model for Flux Measurements in the Convective Boundary Layer

WEIGUO WANG,* KENNETH J. DAVIS, DANIEL M. RICCIUTO, AND MARTHA P. BUTLER

Department of Meteorology, The Pennsylvania State University, University Park, Pennsylvania

(Manuscript received 24 August 2005, in final form 13 February 2006)

ABSTRACT

An explicit footprint model for flux measurements of passive scalars in the lower part of the convective boundary layer (CBL) is introduced. A simple footprint model is derived analytically in an idealized CBL. The simple model can simulate the overall characteristics of the flux footprint. Then a method is proposed to adjust the analytical solutions to those from a Lagrangian stochastic model that considers more realistic atmospheric conditions in the vertical direction. The adjusted footprint model is a function of Monin–Obukhov length (L), roughness length, receptor height, and CBL depth (h). Comparison between the results from the adjusted footprint model and stochastic model suggests that the adjusted footprint model can well simulate the streamwise extent of the footprint within the dimensionless upwind distance $X < 1$, which accounts for a majority of the footprint. The model applies to stabilities of $-L/h$ between 0.01 and 0.1 and roughness lengths between 10^{-5} and $2 \times 10^{-3}h$ in the lower part of the mixed layer (from $0.1h$ to $0.6h$).

1. Introduction

The flux footprint is a measure of the influence of the surface area to a measured vertical turbulent flux (Schuepp et al. 1990) using tower- or aircraft-based eddy covariance methods. The interpretation of eddy covariance flux measurements, for example, over a surface with a heterogeneous source distribution, depends largely on the flux footprint over which the fluxes are sampled. The location and size of the flux footprint for the measurements at a given height, however, usually vary with meteorological conditions and surface conditions. Therefore, it is crucial for designing and interpreting flux measurements to estimate the flux footprint under various conditions.

There are a number of studies about scalar flux footprints for measurements within the surface layer (e.g., Horst and Weil 1992; Schmid 2002; Schuepp et al. 1990). Although horizontally homogeneous atmospheric conditions are usually assumed in most of the current flux footprint models, those models still can provide flux footprint estimates to a first-order approximation over a relatively flat surface (e.g., Amiro 1998; Stoughton et al. 2000). Fluxes have also been measured above the surface layer using aircraft (e.g., Davis et al. 1997; Mahrt 1998; Oncley et al. 1997) and tall-tower (Davis et al. 2003) platforms in order to cover large horizontal distances and observe vertical structure of the atmospheric boundary layer. Under daytime convective conditions, the flux footprint area is usually small for measurements within the surface layer and measured fluxes might not be representative of large areas. In this case, flux measurements at high levels are rather useful. For instance, Davis et al. (2003) proposed an optimal algorithm to estimate the net ecosystem–atmosphere exchange (NEE) of CO_2 from measurements at three levels of a 447-m-tall tower in northern Wisconsin (WLEF), in which nighttime and daytime NEE values are derived primarily from measurements at the lowest level (30 m) and at higher levels (122 and 396 m, usually above the surface layer), respectively. One reason for the combination of the three-level measurements is that the lowest-level measurements with small footprint areas are most likely affected significantly by the tower base in the daytime convective boundary layer (CBL), while higher levels are usually

* Current affiliation: Pacific Northwest National Laboratory, Richland, Washington.

Corresponding author address: Dr. Weiguo Wang, Pacific Northwest National Laboratory, K9-30 Richland, WA 99352.
E-mail: wang@met.psu.edu

decoupled from the earth surface or near the top of the boundary layer at night (Davis et al. 2003). Because of the heterogeneous distribution of forest types in the area, flux footprints for measurements at all levels need to be evaluated in order to interpret the derived NEE on various temporal scales. Such evaluation, however, is still difficult to make currently because flux footprints for measurements above the surface layer have not been extensively studied, unlike those within the surface layer (e.g., without footprints for high-level measurements in the day, footprints for cumulative NEE cannot be estimated on daily or longer time scales). There are a few numerical investigations on footprints for measurements above the surface layer in the CBL, for example, using a stochastic model (Weil and Horst 1992), a large-eddy simulation model (Leclerc et al. 1997), and a second-order closure model (Wang and Davis 2002). None of these models, however, can be used in practice due to the need for substantial computational resources. The goal of this study is to construct an explicit analytical model for practical use in order to quickly estimate flux footprints for measurements above the surface layer in the CBL.

In a similar effort to search for explicit estimates for flux footprints, Kljun et al. (2004) presented a scaling approach that can also simulate footprints for flux measurements from above the surface layer to the middle of the CBL. They constructed a dimensionless footprint function using the Buckingham Π theorem, in which the parameters are determined by fitting the function to the results simulated from a Lagrangian stochastic model. In contrast to their dimensional analysis method, the present study starts with deriving an analytical solution for the flux footprint in an idealized CBL (section 2). Then, the ideal solution is adjusted to major features of the footprint fitted from a Lagrangian stochastic model resulting from very limited field data (section 3), similar to methods used in other studies (Hsieh et al. 2000; Kljun et al. 2004). The limitations of the model are discussed in section 4. We focus on daytime convective conditions for two reasons. First, high-level tower flux measurements are usually not used under nighttime stable conditions (Davis et al. 2003), and aircraft measurements are often made during the daytime (e.g., Davis et al. 1997; Mahrt 1998; Oncley et al. 1997). Second, turbulence structures and parameterizations are relatively better understood under convective conditions than under other conditions. We propose a fast and practical approach to estimating flux footprints for measurements above the surface layer. This work also represents a new application of CBL theories and models.

2. An analytical footprint model under idealized conditions

With zero entrainment flux at the top of CBL, the scalar flux footprint $f(x, y, z_m)$ can be interpreted as the vertical flux downwind of a unit surface point source (Horst and Weil 1992, 1994; Weil and Horst 1992),

$$f(x, y, z_m) = \frac{F_m(x, y, z_m)}{Q}, \tag{1}$$

where x and y are the horizontal distances of the measurement point from a surface point source (sink) with an emission rate Q at the origin, z_m is the measurement height, and $F_m(x, y, z_m)$ is the vertical flux measured at position (x, y, z_m) in the Eulerian field. In Lagrangian models, F_m can be evaluated by recording the trajectories of the particles released from the source into the atmosphere. In the fluid with zero mean vertical velocity, F_m can be written as (van Dop et al. 1985)

$$F_m(x, y, z_m) = \langle w(x, y, z_m) \rangle\, C(x, y, z_m), \tag{2}$$

where $\langle w(x, y, z_m) \rangle$ is an average of the vertical velocities of the released particles passing the infinitesimal small-volume $dxdydz$ centered at (x, y, z_m); $C(x, y, z_m)$ is the mean mixing ratio at position (x, y, z_m), which can be evaluated by counting the number of the trajectories passing the volume.

The crosswind-integrated footprint (CWIF), usually examined in the literature, is defined by

$$f^y(x, z_m) = \int_{-\infty}^{+\infty} f(x, y, z_m)\, dy, \tag{3}$$

and is then

$$f^y(x, z_m) = \frac{F_m^y(x, z_m)}{Q}, \tag{4}$$

where $F_m^y(x, z_m)$ is the crosswind-integrated mean vertical flux that can be derived from Eq. (2) [see Eq. (A1) for the derivation],

$$F_m^y(x, z_m) = \langle w(x, z_m) \rangle\, C^y(x, z_m), \tag{5}$$

where $C^y(x, z_m)$ is the crosswind-integrated mixing ratio.

To obtain an explicit analytical expression for the flux footprint of measurements above the surface layer, dispersion is considered in an idealized CBL with horizontally homogeneous conditions, uniformly distributed horizontal wind speed, vertical velocity skewness, and variance in the vertical direction. In addition, the Lagrangian time scale is assumed to be infinite as adopted in the probability density function (PDF) dispersion models (Luhar 2002; Misra 1982; Weil et al.

1997). This assumption makes use of the observation that the Lagrangian time scale of the convective turbulence is so large that some passive particles tend to remain close to their initial trajectory for a considerable distance. Numerical simulations have justified the assumption indirectly. For example, Weil (1990) simulated the dispersion from a point source at the bottom of the CBL, and found that the large time scale is one of the important reasons for causing the phenomena that the plume rises or "lifts off" the surface as observed both in both the laboratory experiments (Willis and Deardorff 1976) and in field campaigns (Briggs 1993a,b).

With the above assumptions, the initial vertical velocity of an air parcel passing the point (x, z_m) is simply equal to

$$w_p(x, z_m) = \frac{(z_m - z_s)U}{x}, \tag{6}$$

where z_s is the height of the point source, and U is the horizontal wind speed. With multiple perfect reflections on the top and bottom boundaries, by applying Eq. (6) to virtual sources at $z = \pm(2h - z_s)$, $\pm(2h + z_s)$, $\pm(4h - z_s)$, etc., the vertical velocities of all air parcels passing (x, z_m) have the following initial values (Misra 1982; Weil 1988):

$$w_{kj}(x, z_m) = \frac{(2kh + jz_m - z_s)U}{x}, \tag{7}$$

where h is the CBL depth; k is any integer whose absolute value represents the number of times of reflections from the top of CBL; and j is an integer equal to either 1 or -1, indicating reflection on the top or bottom boundaries. The crosswind-integrated mixing ratio contributed by the air parcels with the vertical velocity of w_{kj} is then (Misra 1982; Weil 1988)

$$C^y_{kj}(x, z_m) = Q\frac{p_w(w_{kj})}{x}, \tag{8}$$

where p_w is the probability density function of w_{kj} at the source height. It is usually taken to be the sum of two Gaussian distributions, which provides a good match to observations (Misra 1982; Weil 1988); that is,

$$p_w(w) = \frac{\lambda_1}{\sqrt{2\pi}\sigma_1}\exp\left[-\frac{(w - \overline{w}_1)^2}{2\sigma_1^2}\right] + \frac{\lambda_2}{\sqrt{2\pi}\sigma_2}\exp\left[-\frac{(w - \overline{w}_2)^2}{2\sigma_2^2}\right], \tag{9}$$

where $\lambda_1, \lambda_2, \sigma_1, \sigma_2, \overline{w}_1, \overline{w}_2$ are found by equating the zeroth through the third moments of the assumed distribution with those specified and by assuming that $(\sigma_1/\overline{w}_1) = -(\sigma_2/\overline{w}_2) = R$, a constant. Details on how to determine the six parameters can be found in the literature (e.g., Weil 1990).

For the idealized case we are considering, the Eulerian vertical flux [Eq. (5)] can be written as [see Eq. (A1) for the derivation]

$$F^y_m(x, z_m) = \sum_{j=-1(j\neq 0)}^{+1}\sum_{k=-\infty}^{\infty} w_{kj}(x, z_m)C^y_{kj}(x, z_m). \tag{10}$$

Therefore, the combination of Eqs. (5), (8), (9), and (10) yields an expression of the footprint function according to Eq. (4),

$$f^y(x, z_m) = \begin{cases} \dfrac{1}{x}\displaystyle\sum_{j=-1(j\neq 0)}^{+1}\sum_{k=-\infty}^{\infty} w_{kj}(x, z_m)p_w(w_{kj}), & x > 0 \\ 0, & \text{otherwise,} \end{cases} \tag{11}$$

which is actually a superposition of the functions (with different values of j and k), each of which includes a factor of $\exp(-1/x^2)/x^2$.

Assuming $R = 1$ and $S = 0.5$, typical values in the real CBL, we calculate the footprint as an example (Fig. 1). Taking $|k| = 5$ can provide a sufficient accuracy for the calculation within $X < 4$, where X is the dimensionless upwind distance (w_*x/Uh) and w_* is the convective velocity scale. To characterize the flux footprint, the cumulative footprint (CF) and footprint half-width are introduced in addition to the maximum footprint and its location. The CF is defined as the horizontally integrated footprint,

$$\mathrm{CF}(X, z) = \int_0^X f^y(x, z)\,dx. \tag{12}$$

The equilibrium CF value is referred to the CF value when $X \to +\infty$. The footprint half-width is defined as the horizontal distance between the points where the footprint falls to one-half of its maximum value (Weil and Horst 1992). In the following analyses, the CWIF, footprint half-width, and height are scaled by w_*/Uh, Uh/w_*, and h, respectively.

Figure 1a (solid lines) shows the calculated footprint as a function of X for three measurement heights of 0.1, 0.3, and $0.5h$. The footprint broadens with height, while its peak value decreases with height. These results show general features of the footprint for flux measurements. The equilibrium CF value decreases linearly with height; that is, $\mathrm{CF}(+\infty, z) = 1 - z/h$ (solid line in Fig. 1b). This result is consistent with the linear flux profile

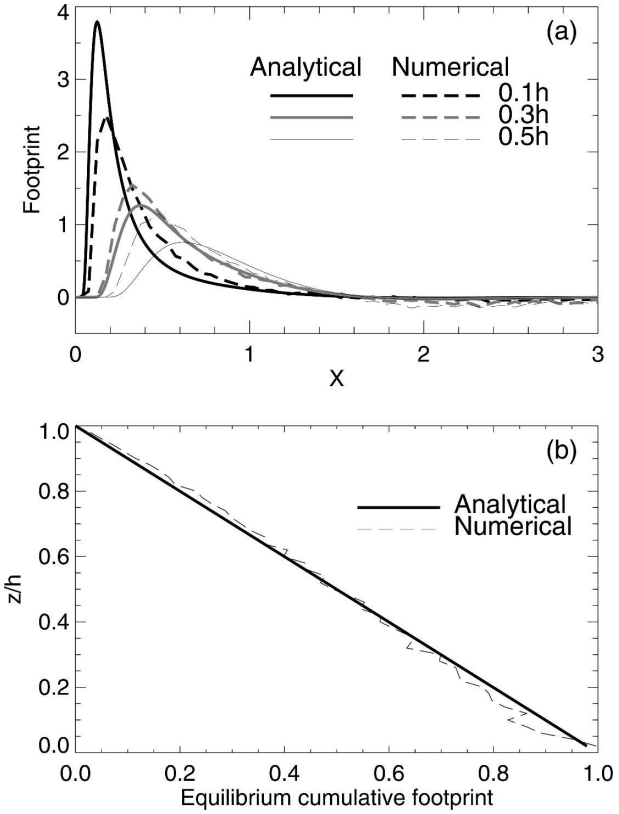

FIG. 1. (a) Normalized crosswind-integrated flux footprint f^y calculated from the idealized model (solid lines) [Eq. (11)] with a vertical velocity skewness of 0.5 and $R = 1$, as a function of the horizontal dimensionless distance (X) from the receptor ($X = 0$) for the measurement heights of 0.1, 0.3, and 0.5h. As a comparison, results from the stochastic model are shown by the dashed lines when $z_0 = 10^{-4}h$ and $L = -0.05h$. Wind direction is from left to right. (b) Height-dependent equilibrium CF($+\infty$, z) values from the idealized model (solid line) and the stochastic model (dashed line).

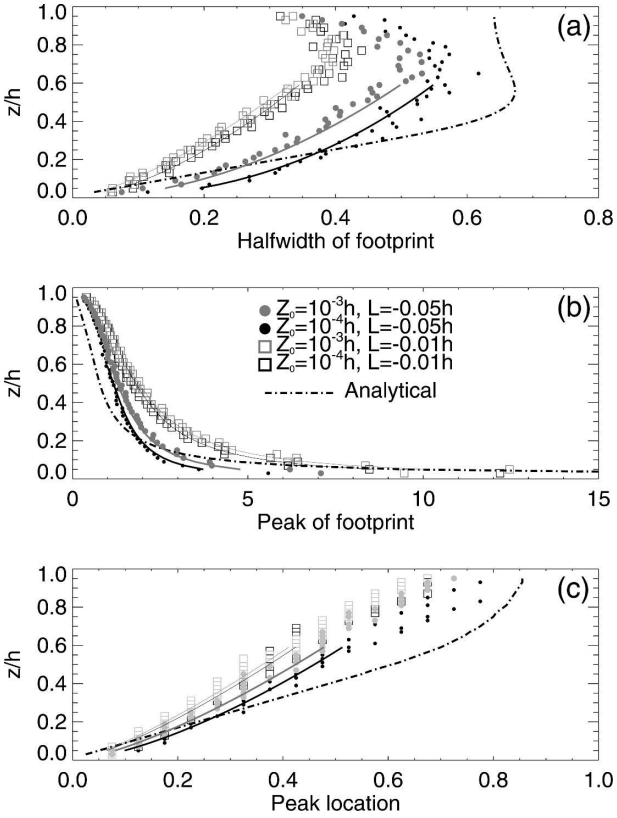

FIG. 2. Normalized (a) half-width, (b) peak, and (c) peak's location of CWIF derived from the idealized model (dot–dash lines) as a function of dimensionless measurement height (z/h). Results from the stochastic model are shown by circles and squares, suggesting the dependence of the quantities on L/h and z_0/h. The solid lines are the fitted lines for the three quantities. Limited horizontal resolution of the stochastic model results in "steps" in (c).

in a well-mixed, horizontally homogeneous boundary layer when the entrainment flux is not considered (Wyngaard and Brost 1984) because the equilibrium value [CF($+\infty$, z)] can be interpreted as the flux at height z above the homogeneous surface with a unit surface flux [see Eq. (12)] according to the footprint definition. This linear relationship also indicates that the surface flux signal becomes weaker as the measurement height increases. The peak value, peak location, and width calculated from Eq. (11) vary with measurement height (dot–dashed lines in Fig. 2).

However, the effects of stability, roughness, and variations in turbulence in the vertical direction are not included in the idealized model. These factors affect the acceleration of air parcels and hence their trajectories, altering footprint simulations. With more realistic wind, temperature, and turbulence profiles, calculation of the footprint function requires numerical evaluation of the air parcel vertical velocities, which is not convenient in practice. Next, we propose a method to adjust Eq. (11) to approximate the more realistic solution of the footprint from a Lagrangian stochastic model.

3. An adjustment for the idealized model

a. Flux footprints evaluated from a Lagrangian stochastic model

The Lagrangian particle model developed by Luhar and Britter (1989) and modified by Luhar et al. (1996) is selected to evaluate the crosswind-integrated vertical flux of the passive scalar released from a surface point source in the CBL, and hence the footprint. The model has been used successfully to simulate the dispersion in the CBL. The results from the model agree well with

those from both water tank experiments (Willis and Deardorff 1976, 1978, 1981) and field observations (Briggs 1993a,b). We slightly modify Luhar and Britter's model by considering the inhomogeneity of the mean horizontal wind profile in the surface layer instead of the uniform wind speed in all levels. The horizontal wind speed is estimated using the Monin–Obukhov surface layer theory below $0.1h$, and is assumed to be uniform with height above $0.1h$. Because the structure of the CBL has been better documented under strongly unstable conditions than under weakly unstable conditions (Weil 1988), only the former conditions, that is, $-h/L > 10$, where L is the Monin–Obukhov length, are considered. The vertical profiles of $\overline{w^2}$ and $\overline{w^3}$ in the CBL summarized by Stull (1988) are used. In the surface layer, we use $(\overline{w^2})^{1/2} = 1.9u_*(-z/L)^{1/3}$ and $\overline{w^3} = 2.5u_*^3(-z/L)$ (Hunt et al. 1988), where u_* is the friction velocity that is related to w_* by $w_*/u_* = (-h/\kappa L)^{1/3}$, and κ is the von Kármán constant. The expressions for $\overline{w^2}$ and $\overline{w^3}$ result in a skewness $S = 0.36$ in the surface layer, consistent with observations (Wyngaard 1988). The surface layer ε is assumed to be $\varepsilon = (u_*^3/\kappa z)[1 + 0.5(-z/L)^{2/3}]^{3/2}$ (Wyngaard and Cote 1971). Reflections are assumed at the bottom and top of the CBL (Weil 1990).

Sixty-three experiments are carried out. The model is run for the cases of $L = -0.01$, -0.02, -0.03, -0.04, -0.05, -0.07 and $-0.09h$, in each of which nine experiments are made with z_0 of 10^{-5}, 3×10^{-5}, 5×10^{-5}, 8×10^{-5}, 10^{-4}, 3×10^{-4}, 5×10^{-4}, 1×10^{-3}, and $2 \times 10^{-3}h$, respectively. Results selected from the cases are shown in Figs. 1 and 2 for comparison with the analytical solutions. The width of the footprint broadens (Fig. 2a), the peak value of the footprint decreases (Fig. 2b), and the peak location of the footprint is farther from the source (Fig. 2c) as the stability increases (larger $|L|$) because the vigor of vertical mixing decreases. A change in the roughness length also affects the features of the footprint. Larger roughness usually indicates stronger mechanically induced turbulent mixing, resulting in a narrower footprint half-width. In all cases, the equilibrium CF linearly decreases with height as shown in Fig. 1b.

The features of the derived footprints can be fitted as functions of measurement height, stability, and roughness length. The dimensionless half-width of the footprint, denoted as $\Delta X_{\text{stochastic}}$, can be described in the lower part of the CBL (less than $0.6h$) by a power-law profile:

$$\Delta X_{\text{stochastic}} = g_1\left(\frac{z}{h}\right)^{g_2}, \tag{13}$$

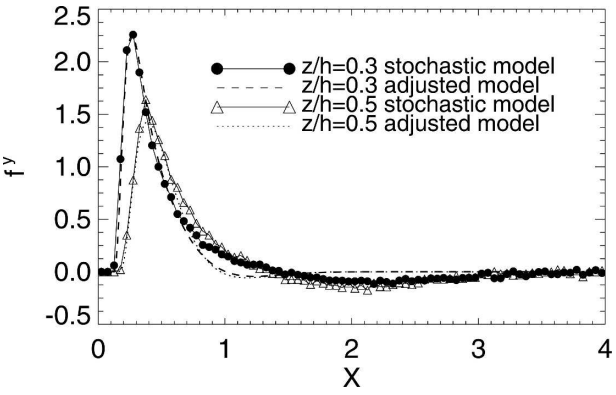

FIG. 3. Comparison of the footprints (CWIF) calculated from the adjusted model and from the stochastic model for measurement heights of 0.3 and $0.5h$ in the case of $L/h = -0.03$ and roughness length $= 1 \times 10^{-3}h$.

where coefficients g_1 and g_2 are polynomial functions of the stability parameter L/h and the dimensionless roughness length z_0/h [Eq. (A5)]. The half-width in the upper part of the CBL is not fitted because the footprint is not well described by this quantity [negative footprint (or flux) values are sizable as the measurement height becomes high, see Figs. 1a and 3; the negative values are attributed to the vertical inhomogeneity of turbulence and large turbulence time scale (Weil and Horst 1992), which is consistent with the finding by Willis and Deardorff (1976) that there is an elevated maximum concentration in the CBL from a surface point source]. In addition, direct measurements of the surface flux should not be made in the upper CBL in practice due to both the weaker surface flux signals and the impact of the entrainment flux.

Similarly, the peak of the footprint, denoted as $F_{\text{max, stochastic}}$, and its location ($X_{\text{max, stochastic}}$) in the lower part of the CBL can be described by

$$F_{\text{max,stochastic}} = g_3\left(\frac{z}{h}\right)^{g_4} + g'\left(\frac{z}{h}\right)^3, \tag{14}$$

and

$$X_{\text{max, stochastic}} = g_5\left(\frac{z}{h}\right)^{g_6}, \tag{15}$$

where g_3, g_4, g_5, g_6, and g' are the coefficients determined by fitting the results from the stochastic model (see appendix). It should be kept in mind that the parameters in Eqs. (13), (14), and (15) apply only when L and z_0 range from -0.01 to $-0.1h$ and from 10^{-5} to $2 \times 10^{-3}h$, respectively. The fitted functions are shown by the solid lines in Fig. 2. These expressions are useful for making a quick estimate of the main features of the footprint given the CBL height, stability, and roughness

length. The streamwise distribution of the footprint can be estimated by adjusting the idealized solution.

b. Adjustment and comparisons

Two parameters are introduced to adjust the main features of the footprint from the idealized model to those from the stochastic model. One, denoted by β, is used to adjust the half-width and peak values of the estimated footprint. The other parameter, γ, is used to adjust the position of the maximum of the footprint by translating the footprint function a distance in the along-wind direction. A necessary condition that the equilibrium cumulative footprints of the adjusted and nonadjusted models are equal at the same height is imposed; that is,

$$\int_0^{+\infty} f_a^y(x, z_m)\, dx = \int_0^{+\infty} f^y(x, z_m)\, dx = 1 - \frac{z_m}{h}, \tag{16}$$

where $f_a^y(x, z_m)$ is the adjusted footprint function, which, therefore, can be written as

$$f_a^y(x, z_m) = \begin{cases} \beta \dfrac{F_m^y(\beta x + \gamma, z_m)}{Q} = \\ \displaystyle\sum_{j=-1(j\neq 0)}^{+1} \sum_{k=-\infty}^{\infty} \beta \frac{w_{kj}(\beta x + \gamma, z_m) p_w[w_{kj}(\beta x + \gamma, z_m)]}{\beta x + \gamma}, \\ \text{for} \quad \min[\beta x + \gamma, x] > 0 \\ 0, \qquad\qquad\qquad\qquad\qquad\qquad \text{otherwise,} \end{cases} \tag{17}$$

where β is a function of stability, roughness length, and height; it can be calculated by

$$\beta = \alpha \frac{\Delta X_{\text{ideal}}}{\Delta X_{\text{stochastic}}} + (1 - \alpha) \frac{F_{\text{max, stochastic}}}{F_{\text{max, ideal}}}, \tag{18}$$

where α is a coefficient determining the relative adjustment weight. The parameter γ is calculated by

$$\gamma = X_{\text{max, ideal}} - \beta X_{\text{max, stochastic}}, \tag{19}$$

where ΔX_{ideal}, $F_{\text{max, ideal}}$, and $X_{\text{max, ideal}}$ are the half-width, peak, and peak location of the CWIF as determined from the idealized model [see Eqs. (A6)–(A8)]. The appendix shows that the adjusted function Eq. (17) can satisfy the constraint Eq. (16) for a broad range of typical roughness lengths and atmospheric stabilities.

After adjustment, the analytical solution is generally in good agreement with that from the stochastic model. Figure 3 shows the comparison of the CWIFs obtained from the stochastic model and the adjusted model for two measurement heights $z = 0.3h$ and $z = 0.5h$ under the conditions of $L = -0.03h$ and $z_0 = 10^{-3}h$. The coefficient α is taken as 0.5, suggesting equal weights of the width and the peak of the footprint in the adjustment calculation. In the lower CBL ($0.3h$), results from the adjusted model agree well with that from the stochastic model in the range of $0 < X < 1$, which accounts for the majority of the footprint. For the higher altitude ($0.5h$), the adjusted model predicts a more rapid decrease in the footprint to the right of the peak than the stochastic model despite good agreement in the range of $X < 0.65$. The performance of the adjusted model is poor far away from the receptor, that is, $X > 1$ or 2, due to oversimplified physics. The negative footprint and its location are not well simulated in the adjusted model, particularly under strongly unstable conditions or at high measurement levels. Nevertheless, the model still can be used to estimate the footprint in the lower levels of the CBL because the portion of the footprint in the range of $X > 1$ is small ($\sim$10%).

We compared the flux footprints estimated from the explicit model by Kljun et al. (2004) and the adjusted footprint model in this study at three receptor heights above the surface layer for L values of $-0.03h$ and $-0.07h$ with $z_0 = 10^{-4}h$ (Fig. 4). The estimated footprints from the two models are qualitatively consistent in terms of their dependences on the roughness length, stability, and the receptor height. Quantitatively, the differences in the peak, peak location, and the width of the footprint are significant. In addition, the model by Kljun et al. (2004) predicts small contributions of the footprints downwind of the receptor (i.e., $X < 0$), which is not predicted in the adjusted model. The significant differences are most likely due to the different stochastic models used to calibrate the explicit models. The parameters in the model by Kljun et al. (2004) are fitted by the results from a stochastic model with the effects of the longitudinal turbulence being considered. Along-wind turbulence is not considered in the numerical model we used, which is a major simplification. The uncertainty of the adjusted model is closely related to that of the numerical model results. It should be remembered that results from other numerical models or

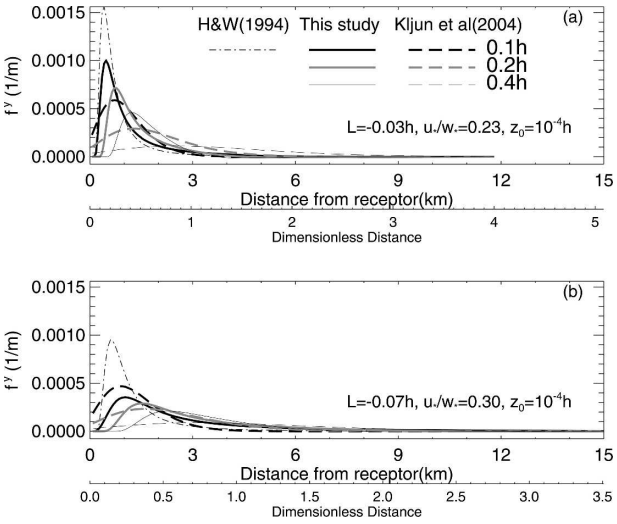

FIG. 4. Comparison of the estimated CWIFs from the adjusted model of this study [Eq. (17)] (solid lines) and from the empirical model (broken lines) by Kljun et al. (2004) at three heights above the surface layer with (a) $L = -0.03h$ and (b) $L = -0.07h$ for $z_0 = 10^{-4}h$. The dot–dash lines are the results at the top of the surface layer ($0.1h$) from the analytical surface layer model by Horst and Weil (1994).

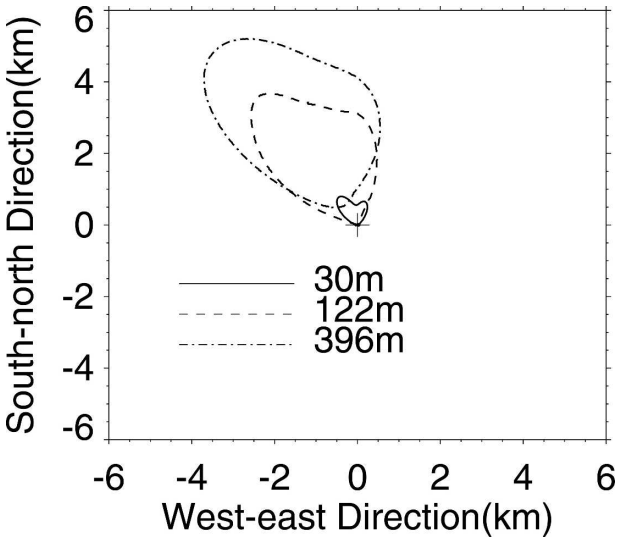

FIG. 5. The 80% surface source (sampling) areas for flux measurements at three heights of 30, 122, and 396 m, respectively. The cross represents the location of the tower. The three lines represent the 80% surface source area boundaries, estimated using the averaged footprint with meteorological conditions measured at the WLEF tower from 0900 to 1700 local time 4 Jun 1998. A dynamically homogeneous surface is assumed in this example.

observations could also be used to adjust our explicit model. Flux footprints for measurements at the top of the surface layer ($0.1h$) are also evaluated using the analytical model derived by Horst and Weil (1992, 1994); the flux footprint peak is higher, the peak location is closer to the receptor, and streamwise extension is smaller as compared to the other two models (Fig. 4) because the mean plume height is likely overestimated at high altitudes based on the surface layer turbulence (Weil and Horst 1992). This comparison suggests that applying a surface layer footprint model to measurements above the surface layer may result in significant errors.

c. An example

Flux footprints are estimated for measurements within and above the surface layer as an example (Fig. 5). Meteorological conditions are taken from measurements at the 447-m-tall tower during the daytime on 4 June 1998. Dominant wind directions are north-northwest and north-northeast from 0900 to 1400 and from 1400 to 1700 local time, respectively. CBL heights measured from a 915-MHz boundary layer profiling radar (Yi et al. 2001) vary from 1500 to 2300 m. The L values range from -200 to -100 m. The roughness length and zero-plane displacement height are assumed to be 0.1 and 10 m, respectively. In the lateral direction, the footprint is assumed to be a Gaussian distribution (Horst and Weil 1992), that is,

$$f(x, y, z_m) = f^y(x, z_m)\frac{1}{\sqrt{2\pi}\sigma_y}\exp\left(-\frac{y^2}{2\sigma_y^2}\right), \tag{20}$$

where σ_y is the standard deviation of the plume in the lateral direction. To a first approximation, $\sigma_y = 0.32x(1 + 0.0004x)^{-1/2}$ (Arya 1999). The analytical model developed by Horst and Weil (1992, 1994) is used to estimate the crosswind-integrated footprint for measurements within the surface layer, and the adjusted footprint model developed in this paper is used for measurements above the surface layer.

Figure 5 shows the mean surface source areas evaluated from footprints for the measurements at three heights (30, 122, and 396 m), suggesting significant differences in sampling areas. The three lines in the figure are the contours of the footprints averaged from 0900 to 1700 local time, enclosing 80% of the surface source areas for the measurements at the three heights, respectively. In other words, the integrated footprint over each enclosed surface source area (where the footprint values are greater than the value represented by the corresponding contour) is 80% of the total integrated footprint over the infinite area in this case (Amiro 1998; Schmid 2002).

4. Summary and discussion

An analytical model for flux footprints in an idealized CBL is derived based on existing CBL theories and

models. The idealized model can capture the overall characteristics of the footprint function simulated from the stochastic model. Because of the assumptions simplifying the model, the dependence of the footprint on stability and roughness is not reflected in the simple model. Our goal is to develop an explicit analytical footprint model that can be as accurate as possible and can be efficiently used in practice. To this end, the idealized footprint model is adjusted to more closely match the main features derived from a Lagrangian stochastic model with state-of-the-art vertical turbulence parameterizations. The solutions from the adjusted model are in good agreement with those from the stochastic model for $X < 1$, which covers the majority of the footprint. Applying a surface layer model to measurements above the surface layer in the CBL would result in significant errors in predicting the peak, peak location, and extent of the footprint.

It should be noted that there are limitations of the adjusted flux footprint model.

- The model can be used only below 60% of the CBL depth because the fit is only accurate below $0.6h$. In addition, the effect of entrainment on the footprint, more significant with increasing height, is not considered in either the stochastic or the idealized footprint models. In reality, measuring surface fluxes far away from the surface yields very little information about the surface flux.
- The model applies to stabilities of $0.01 < -L/h < 0.1$ and roughness lengths of $10^{-5} < z_0/h < 2 \times 10^{-3}$, where the model is empirically adjusted. Under extremely unstable conditions, the effects of the alongwind turbulence would be significant and are not considered in our adjusted model.
- Researchers should avoid using the adjusted model close to the surface ($z_m < 0.05h$). The main features of the footprint are better represented by the fitted curves above the surface layer than within the surface layer, because few data points below the surface layer are fitted.
- The model applies only over a dynamically homogeneous surface like other analytical footprint models in the literature.
- The negative footprint, which is more significant with height and found at a distance of approximately $X > 1$ or 2, is not well simulated by the adjusted model. Because only a small portion of the total footprint is contributed by the range $X > 2$, the adjusted model still can accurately simulate the main features of the footprint above the surface layer in the lower part of CBL.

Despite the limitations, the analytical solution renders the adjusted footprint model very convenient to use in practice. The explicit model runs much faster (e.g., $>10^3$–10^5 times) than numerical models, such as stochastic and large-eddy simulation models, and, therefore, it can be used for estimating footprints in days and years as long as the model's applicable conditions are met.

The present model can be improved by considering more physics and can be better-adjusted based on direct footprint measurements or simulations from more realistic models or using other adjustment methods. The applicability of the model may be expanded if reliable flux footprint results under other unstable conditions or under other surface roughness conditions are available. In addition, measurements are needed to make further assessments about the accuracy of the existing numerical models and to improve the ability of footprint simulations because the accuracy of the adjusted model depends partially on the simulation results.

Acknowledgments. We thank Dr. A. Luhar who provided the source code of the Lagrangian stochastic model used in this study. This research was supported in part by National Science Foundation Research Collaboration Network Grant DEB-0130380, and the Office of Science, U.S. Department of Energy (DOE) through Terrestrial Carbon Processes Program and NIGEC. Any opinions, findings, and conclusions or recommendations herein are those of the authors and do not necessarily reflect the views of the DOE or the NSF. The carbon dioxide mixing ratio measurements and site infrastructure at WLEF were supported by the Atmospheric Chemistry Project of the Climate and Global Change Program of the National Oceanic and Atmospheric Administration. Work at the WLEF television tower would not be possible without the gracious cooperation of the Wisconsin Educational Communications Board and R. Strand, chief engineer for WLEF-TV. We thank two reviewers for their constructive comments and suggestions.

APPENDIX

Some Derivations

a. Expression of the vertical turbulent flux

Following the derivation by van Dop et al. (1985), we can write the mean vertical flux of the mixing ratio of a scalar in a fluid with zero mean vertical flow in the Eulerian field as, by definition,

$$\overline{\tilde{w}\tilde{c}}(x, y, z) = \frac{1}{N}\sum_{i=1}^{N} \tilde{w}_i(x, y, z)\tilde{c}_i(x, y, z), \quad \text{(A1)}$$

where N is the total number of the fluid particles passing though an infinitesimally small volume centered at point (x, y, z); $\tilde{w}_i$ and $\tilde{c}_i$ are instantaneous values of vertical velocity and mixing ratio, respectively. Of the particles, only a subensemble of M ($M \le N$) particles has passed through the source z_s with a constant mixing ratio q, and hence the mixing ratio at the point is $C(x, y, z) = qM/N$. Because $\tilde{c}_i$ is only nonzero (equal to q) for the particles having passed the source, Eq. (A1) reduces to

$$\overline{\tilde{w}\tilde{c}}(x, y, z) = \frac{q}{N}\sum_{i=1}^{M} \tilde{w}_i(x, y, z) = \left[\frac{1}{M}\sum_{i=1}^{M} \tilde{w}_i(x, y, z)\right]\frac{qM}{N} = \langle w(x, y, z)\rangle\, C(x, y, z), \quad \text{(A2)}$$

where $\langle w(x, y, z)\rangle$ is the mean vertical velocity of the M particles. Equation (A2) was shown by van Dop et al. (1985).

In the two-dimensional case, Eq. (A2) can be reduced to

$$\overline{\tilde{w}\tilde{c}}(x, z) = \frac{q}{N}\sum_{i=1}^{M'} \tilde{w}_i(x, z) = \left[\frac{1}{M'}\sum_{i=1}^{M'} \tilde{w}_i(x, z)\right]q\frac{M'}{N} = \langle w(x, z)\rangle\, C(x, z), \quad \text{(A3)}$$

where $\langle w(x, z)\rangle$ is the mean vertical velocity of the M' (obviously, $M' \ge M$) particles passing through the source and point (x, z); $C(x, z)$ is the mixing ratio at point (x, z), which is equivalent to the y-direction integrated mixing ratio and is usually written as $C^y(x, z)$.

For the special case in section 2 where the vertical velocities of the air parcels passing the source can be explicitly expressed as n discrete values, such as $\tilde{w}_1$, $\tilde{w}_2, \ldots, \tilde{w}_n$, Eq. (A2) or (A3) can be rewritten as

$$\overline{\tilde{w}\tilde{c}} = \frac{q}{N}\sum_{i=1}^{M} \tilde{w}_i = \frac{q}{N}\sum_{i=1}^{n} n_i\tilde{w}_i = \sum_{i=1}^{n} \tilde{w}_i\frac{q}{N}n_i = \sum_{i=1}^{n} \tilde{w}_i C_i, \quad \text{(A4)}$$

where C_i and $C_i\tilde{w}_i$ are the mixing ratio and the vertical flux, respectively, contributed by the n_i ($\Sigma_{i=1}^{n} n_i = M$) air parcels with the vertical velocity of $\tilde{w}_i$. Equation (A4) yields the result, that is, Eq. (10).

b. Coefficients in the fitted curves

The dimensionless $\Delta X_{\text{stochastic}}$, $F_{\text{max,stochastic}}$, and $X_{\text{max,stochastic}}$ are fitted as Eqs. (13), (14), and (15), where the coefficients are dependent on the stability (L/h) and roughness length (z_0/h). The coefficients are fitted using the following polynomial function:

$$g_k\left(\frac{L}{h}, \frac{z_0}{h}\right) = a_k(0) + a_k(1)\frac{L}{h} + a_k(2)\frac{z_0}{h} + a_k(3)\frac{L}{h}\frac{z_0}{h} + a_k(4)\left(\frac{L}{h}\right)^2 + a_k(5)\left(\frac{z_0}{h}\right)^2, \quad \text{(A5)}$$

where g_k represents the kth coefficient in the equations, and k is from 1 to 6; the values of a_k (0:5) are the fitted coefficients for g_k. The coefficients of determination (r^2) for the fitted curves are greater than 0.95.

For Eq. (13), $\Delta X_{\text{stochastic}} = g_1((z/h))^{g_2}$,

$a_1 = [0.41, -7.07, 12.53, 959.65, -30.45, 0.00]$;

$a_2 = [0.67, 5.08, 97.26, -62.77, 0.00, 0.00]$.

For Eq. (14), $F_{\text{max, stochastic}} = g_3((z/h))^{g_4} + g'((z/h))^3$,

$a_3 = [1.33, 11.24, 11.53, -500.30, 7.89, 0.00]$;

$a_4 = [-0.69, -4.78, 45.59, 679.85, 0.00, 0.00]$, and $g' = -0.95$.

For Eq. (15), $X_{\text{max, stochastic}} = g_5((z/h))^{g_6}$,

$a_5 = [0.61, -1.97, -9.80, 494.18, 7.89, 0.00]$;

$a_6 = [0.78, 2.45, 13.44, -915.30, 0.00, 0.00]$.

With the parameters used ($R = 1$, $S = 0.5$) in this study, ΔX_{ideal}, $X_{\text{max, ideal}}$, and $F_{\text{max,ideal}}$ for the idealized model [Eq. (11)] can be fitted by the following curves:

$$\Delta X_{\text{ideal}} = \sum_{i=1}^{5} d_i\left(\frac{z}{h}\right)^i, \quad \text{(A6)}$$

where d_i ($I = 1$–5) is the coefficient of the fitted polynomial function; $d = [1.131, 5.7192, -17.822, 17.058, -5.4377]$;

$$X_{\text{max, ideal}} = 1.2305\left(\frac{z}{h}\right)^{0.993} \quad \text{for} \quad z \le 0.6h, \quad \text{(A7)}$$

and

$$f_{\text{max, ideal}} = 0.3766\left(\frac{z}{h}\right)^{-1.0028} \quad \text{for} \quad z \le 0.6h. \quad \text{(A8)}$$

The coefficients of determination (r^2) for the fitted curves are greater than 0.99.

c. Examining Eq. (16)

The condition Eq. (16) is examined as follows:

$$\int_0^{+\infty} f_a^y(x, z_m)\, dx = \int_0^{+\infty} \beta f^y(\beta x + \gamma, z_m)\, dx. \tag{A9}$$

Let

$$x' = \beta x + \gamma. \tag{A10}$$

Equation (A9) becomes

$$\int_0^{+\infty} f_a^y(x, z_m)\, dx = \int_\gamma^{+\infty} f^y(x', z_m)\, dx' = \int_0^{+\infty} f^y(x, z_m)\, dx - \int_0^{\gamma} f^y(x, z_m)\, dx. \tag{A11}$$

The second integral on the far right-hand side of Eq. (A11) is equal to zero if $\gamma \le 0$ according to Eq. (11). In this case, the constraint [Eq. (16)] is satisfied. If $\gamma > 0$, the second integral is nonzero. For a small γ, the integral can be negligible because the footprint near the source may be close to zero. Calculation suggests that the integral is significant only when z_m is small (e.g., less than $0.02h$). In this case, the position of the footprint peak is close to the receptor. For the cases above the surface layer, the integral is negligible. Therefore, the constraint Eq. (16) is approximately satisfied for the range of height where the model is applicable.

The case of $\gamma > 0$ indicates that surface sources downwind of the receptor ($x < 0$, note that the wind comes from left to right) could contribute to the measured flux. In particular, for the measurements close to the surface under extremely unstable conditions, such contribution could be significant due to the effect of the along-wind turbulence, which is also shown by numerical studies (Kljun et al. 2002, 2003). In this case, with the inclusion of the footprint at negative x, the integral in the constraint Eq. (16) is rewritten as

$$\int_{-\infty}^{+\infty} f_a^y(x, z_m)\, dx = \int_{-\infty}^{+\infty} f^y(x, z_m)\, dx = 1 - \frac{z_m}{h}, \tag{A12}$$

and the adjusted footprint model Eq. (17) can be rewritten accordingly as

$$f_a^y(x, z_m) = \begin{cases} \displaystyle\sum_{j=-1(j\neq 0)}^{+1} \sum_{k=-\infty}^{\infty} \beta \frac{w_{kj}(\beta x + \gamma, z_m) p_w[w_{kj}(\beta x + \gamma, z_m)]}{\beta x + \gamma}, \\ \text{for} \quad x > \min\left[-\dfrac{\gamma}{\beta}, 0\right] \\ 0, \qquad\qquad \text{otherwise}, \end{cases} \tag{A13}$$

where the contribution of the surface sources downwind of the receptor is considered. In this case, Eq. (A13) exactly meets Eq. (A12).

REFERENCES

Amiro, B. D., 1998: Footprint climatologies for evapotranspiration in a boreal catchment. *Agric. For. Meteor.,* **90,** 195–201.

Arya, S. P., 1999: *Air Pollution Meteorology and Dispersion*. Oxford University Press, 310 pp.

Briggs, G. A., 1993a: Plume dispersion in the convective boundary layer. Part II: Analyses of CONDORS field experiment data. *J. Appl. Meteor.,* **32,** 1388–1425.

——, 1993b: Final results of the CONDORS convective diffusion experiment. *Bound.-Layer Meteor.,* **62,** 315–328.

Davis, K. J., G. Ehret, A. Giez, J. Mann, D. H. Lenschow, S. P. Oncley, and C. Kiemle, 1997: Role of entrainment in surface-atmosphere interactions over the boreal forest. *J. Geophys. Res.,* **102,** 29 219–29 230.

——, P. S. Bakwin, C. Yi, B. W. Berger, C. Zhao, R. M. Teclaw, and J. G. Isebrands, 2003: The annual cycles of CO_2 and H_2O exchange over a northern mixed forest as observed from a very tall tower. *Global Change Biol.,* **9,** 1278–1293.

Horst, T. W., and J. C. Weil, 1992: Footprint estimation for scalar flux measurements in the atmospheric surface layer. *Bound.-Layer Meteor.,* **59,** 279–296.

——, and ——, 1994: How far is far enough? The fetch requirements for micrometeorological measurement of surface fluxes. *J. Atmos. Oceanic Technol.,* **11,** 1018–1025.

Hsieh, C.-I., G. Katul, and T.-W. Chi, 2000: An approximate analytical model for footprint estimation of scalar fluxes in thermally stratified atmospheric flows. *Adv. Water Res.,* **23,** 765–772.

Hunt, J. C. R., J. C. Kaimal, and J. E. Gaynor, 1988: Eddy structure in the convective boundary layer—New measurements and new concepts. *Quart. J. Roy. Meteor. Soc.,* **114,** 827–858.

Kljun, N., M. W. Rotach, and H. P. Schmid, 2002: A three-dimensional backward Lagrangian footprint model for a wide range of boundary-layer stratifications. *Bound.-Layer Meteor.,* **103,** 205–226.

——, R. Kormann, M. W. Rotach, and F. X. Meixer, 2003: Comparison of the Langrangian footprint model LPDM-B with an analytical footprint model. *Bound.-Layer Meteor.,* **106,** 349–355.

——, P. Calanca, M. W. Rotach, and H. P. Schmid, 2004: A simple parameterisation for flux footprint predictions. *Bound.-Layer Meteor.,* **112,** 503–523.

Leclerc, M. Y., S. Shaohua, and B. Lamb, 1997: Observations and large-eddy simulation modeling of footprints in the lower convective boundary layer. *J. Geophys. Res.,* **102,** 9323–9334.

Luhar, A. K., 2002: The influence of vertical wind direction shear on dispersion in the convective boundary layer, and its incorporation in coastal fumigation models. *Bound.-Layer Meteor.,* **102,** 1–38.

——, and R. E. Britter, 1989: A random walk model for dispersion in inhomogeneous turbulence in a convective boundary layer. *Atmos. Environ.,* **23,** 1911–1924.

——, M. F. Hibberd, and P. J. Hurley, 1996: Comparison of closure schemes used to specify the velocity PDF in Lagrangian stochastic dispersion models for convective conditions. *Atmos. Environ.,* **30,** 1407–1418.

Mahrt, L., 1998: Flux sampling errors for aircraft and towers. *J. Atmos. Oceanic Technol.,* **15,** 416–429.

Misra, P. K., 1982: Dispersion of non-buoyant particles inside a convective boundary layer. *Atmos. Environ.,* **16,** 239–243.

Oncley, S. P., J. Mann, D. H. Lenschow, T. L. Campos, and K. J. Davis, 1997: Regional-scale surface flux observations across the boreal forest during BOREAS. *J. Geophys. Res.,* **102,** 29 147–29 154.

Schmid, H. P., 2002: Footprint modeling for vegetation atmosphere exchange studies: A review and perspective. *Agric. For. Meteor.,* **113,** 159–183.

Schuepp, P. H., M. Y. Leclerc, J. I. Macpherson, and R. L. Desjardins, 1990: Footprint prediction of scalar fluxes from analytical solutions of the diffusion equation. *Bound.-Layer Meteor.,* **50,** 355–373.

Stoughton, T. E., D. R. Miller, X. Yang, and G. M. Hendrey, 2000: Footprint climatology estimation of potential control ring contamination: At the Duke Forest FACTS-1 experiment site. *Agric. For. Meteor.,* **100,** 73–82.

Stull, R. B., 1988: *An Introduction to Boundary Layer Meteorology.* Kluwer Academic, xii + 666 pp.

van Dop, H., F. T. M. Nieuwstadt, and J. C. R. Hunt, 1985: Random walk models for particle displacements in inhomogeneous unsteady turbulent flows. *Phys. Fluid,* **28,** 1639–1659.

Wang, W., and K. J. Davis, 2002: Influences of surface heterogeneity on tower-based flux measurements. Preprints, *15th Symp. on Boundary Layers and Turbulence,* Wageningen, Netherlands, Amer. Meteor. Soc., 121–124.

Weil, J. C., 1988: Dispersion in the convecetive boundary layer. *Lectures on Air Pollution Modeling,* A. Venkatram and J. C. Wyngaard, Eds., Amer. Meteor. Soc., 167–221.

——, 1990: A diagnosis of the asymmetry in top-down and bottom-up diffusion using a Lagrangian stochastic model. *J. Atmos. Sci.,* **47,** 501–515.

——, and T. W. Horst, 1992: Footprint estimates for atmospheric flux measurements in the convective boundary layer. *Precipitation Scavenging and Atmosphere-Surface Exchange,* S. E. Schwartz and W. G. N. Slinn, Eds., Hemisphere, 717–728.

——, L. A. Corio, and R. P. Brower, 1997: A PDF dispersion model for buoyant plumes in the convective boundary layer. *J. Appl. Meteor.,* **36,** 982–1003.

Willis, G. E., and J. W. Deardorff, 1976: A laboratory study of diffusion into the convective planetary boundary layer. *Quart. J. Roy. Meteor. Soc.,* **102,** 727–745.

——, and ——, 1978: A laboratory study of dispersion from an elevated source within a modeled convective planetary boundary layer. *Atmos. Environ.,* **12,** 1305–1311.

——, and ——, 1981: Laboratory study of dispersion from a source in the middle of the convectively mixed layer. *Atmos. Environ.,* **15,** 109–117.

Wyngaard, J. C., 1988: Structure of PBL. *Lectures on Air Pollution Modeling,* A. Venkatram and J. C. Wyngaard, Eds., Amer. Meteor. Soc., 9–61.

——, and O. R. Cote, 1971: The budgets of turbulent kinetic energy and temperature variance in the atmospheric surface layer. *J. Atmos. Sci.,* **28,** 190–201.

——, and R. A. Brost, 1984: Top-down and bottom-up diffusion of a scalar in the convective boundary layer. *J. Atmos. Sci.,* **41,** 102–112.

Yi, C., K. J. Davis, B. W. Berger, and P. S. Bakwin, 2001: Long-term observations of the dynamics of the continental planetary boundary layer. *J. Atmos. Sci.,* **58,** 1288–1299.